

**Project: Solar Orbiter SWA**

**Submitted by:** C J Owen

**TITLE:** SWA EAS – Caveats to use of Science Data Products

**Document Number:** SO-SWA-MSSL-TN-015 **Issue:** 1

**Date:** 1<sup>st</sup> December 2020

Author:

\_\_\_\_\_ SWA Ops Team \_\_\_\_\_ Date: \_\_\_\_\_ 1/12/2020 \_\_\_\_\_

Manager/Project Office:

\_\_\_\_\_ Date: \_\_\_\_\_

PA:

\_\_\_\_\_ Date: \_\_\_\_\_

**Distribution:**

Mullard Space Science	C J Owen	X	LPP	M Berthomier	X
Laboratory	C Brockley-Blatt	X			
	D Kataria	X	IAPS	R Bruno	X
	G Lewis	X		F Marcucci	X
	G Watson	X			
	C Anekallu	X	Planetek	L Amoruso	X
	C Kelly	X		V Fortunato	X
	A Mayall	X			
	S Gradone	X	Northumbria	R Wicks	X
	D Verscharen	X			
	L Bercic	X			



**CHANGE RECORD**

ISSUE	DATE	PAGES CHANGED	COMMENTS
1	01/12/2020	All new	First version



## CONTENTS

<b>1</b>	<b>Authors .....</b>	<b>5</b>
<b>2</b>	<b>Introduction .....</b>	<b>5</b>
2.1	<b>Purpose.....</b>	<b>5</b>
<b>3</b>	<b>Normative references .....</b>	<b>5</b>
<b>4</b>	<b>SWA EAS 3d Distributions .....</b>	<b>7</b>
4.1	<b>Angle / Field-of-View effects .....</b>	<b>7</b>
4.2	<b>Energy range .....</b>	<b>10</b>
4.3	<b>The ‘Sawtooth’ .....</b>	<b>10</b>
<b>5</b>	<b>Onboard Moments .....</b>	<b>11</b>
5.1	<b>Executive Summary Statement: .....</b>	<b>11</b>
5.2	<b>General discussion of EAS moments .....</b>	<b>11</b>
5.3	<b>Practicalities of constructing L2 Moments from L1 onboard partial moments.....</b>	<b>13</b>
5.3.1	<b>Cross calibration of the sensor heads.....</b>	<b>13</b>
5.3.2	<b>Density Moment.....</b>	<b>15</b>
5.3.3	<b>Velocity Moments .....</b>	<b>16</b>
5.3.4	<b>Heat Flux Vector Moments .....</b>	<b>18</b>
5.3.5	<b>Pressure Moments.....</b>	<b>18</b>
<b>6</b>	<b>Burst Mode .....</b>	<b>19</b>
	<b>Appendix A – Moment Calculations .....</b>	<b>20</b>
	<b>Appendix B: Abbreviations .....</b>	<b>22</b>

## 1 Authors

This document contains contributions from a number of authors within the SWA-EAS team, including:

Robert T. Wicks<sup>1,2</sup>, George Nicolaou<sup>3</sup>, Christopher Owen<sup>2</sup>, Dhiren Kataria<sup>2</sup>, Chandrasekhar Anekallu<sup>2</sup>, Gethyn Lewis<sup>2</sup>, Matthieu Berthomier<sup>4</sup>, Laura Bercic<sup>2</sup>, Chris Kelly<sup>2</sup>, Vito Fortunato<sup>4</sup>.

<sup>1</sup> Northumbria University, Newcastle-upon-Tyne, <sup>2</sup> UCL Mullard Space Science Lab., Dorking, <sup>3</sup> South-West Research Institute, Texas, USA, <sup>4</sup> LPP, Paris, France, <sup>4</sup> Planetek Italia S.r.l., Bari, Italy.

## 2 Introduction

This document describes the data from SWA/EAS on Solar orbiter and particularly the artefacts affecting the data and the resultant caveats for their use. EAS data are provided in the form of on-board calculated moments, on ground calculated moments and as 3D distributions reported in counts and in distribution function format. These data are calculated from raw counts based on the on-ground and in-flight calibration of the two top-hat analyzers.

At first release (Dec 2020) much of the data is still in need of further analysis, correction and validation for these effects, so the user should take them as caveat emptor, particularly if these are being used in the absence of SWA team advice. Users should contact Chris Owen ([c.owen@ucl.ac.uk](mailto:c.owen@ucl.ac.uk)) to discuss science use and/or to arrange work with improved analysis for particular periods of interest. It is anticipated that this is a 'living' document that will evolve as improvements in the data products are made and released to the data archive. The user is thus encouraged to consult this page for updates on a regular basis.

### 2.1 Purpose

The purpose of this documents is to provide a summary of the SWA/EAS data products and the caveats for use. Full details of the instrument can be found in NR1, although short summaries are given here. The following sections describe caveats and observations made by the instrument team during the commissioning and first months of cruise phase observations. This document is intended to help those using the EAS data for scientific purposes by describing the as-yet uncalibrated artifacts, discrepancies and other features of note in the data. This document is not an exhaustive list and we stress again that any feature in the data that users find that seems unexpected should be discussed with the PI ([c.owen@ucl.ac.uk](mailto:c.owen@ucl.ac.uk)) before it is used for scientific analysis and publication.

## 3 Normative references

This document incorporates, by dated or undated reference, provisions from the following publications.

Ref.	No	Title
NR1	doi:10.1051/0004-6361/201937259	SWA Instrument Paper - The Solar Orbiter Solar Wind Analyser (SWA) Suite, C.J. Owen et al., A&A, August 2020.
NR2	SO-SWA-MSSL-RQ-010	Scientific Operations Algorithms and Processes
NR3	pks105-39-3.1	Solar Orbiter SWA Data Processing Unit - Scientific Algorithms Performance Analysis
NR4	doi:10.1051/0004-6361/201937257	MAG instrument paper - The Solar Orbiter magnetometer, T.S. Horbury et al., A&A, August 2020.

## 4 SWA EAS 3d Distributions

Issues described for the 3D distribution will also affect the moment calculations described below.

### 4.1 Angle / Field-of-View effects

Azimuth bins are fixed by the location of anodes in the detector; however, the elevation angle is controlled by electrostatic deflection. The deflection is caused by voltage applied to plates at the aperture of the instrument. The elevation sweep was changed slightly on 27<sup>th</sup> August 2020 and so data from before and after this date must be treated slightly differently. It is therefore essential to use the elevation table given in each data file separately.

#### Angle acceptance for each deflection state.

The deflection states are not equally spaced across the 90-degree field-of-view for elevation on each detector. The reason for this is that as the deflection increases so does the acceptance angle of the detector, i.e. electrons from a wider range of angles are counted when the deflection angle is larger. The spacing of the deflection states is designed, based on on-ground calibration, to ensure an even coverage of the sky in terms of sensitivity of the instrument, ensuring that there is not 'double counting' or low-count 'gaps' in the distribution.

Data recorded before 27<sup>th</sup> August 2020 therefore have a different distribution on the sky, that includes small patches of overlap and gaps. Moments calculated from data before and after 27<sup>th</sup> August 2020 will have a small systematic difference due to the change of deflection settings.

#### Field-of-View

The FoV of EAS includes several mechanical blockages that reduce count rates. Blockages caused by the EAS design are included in the calibration of distribution function from counts, and so their effect on distribution function is small (although can still be detected). Blockages caused by the spacecraft could not be calibrated before launch and so are still present in the data, we describe some of these below. Some spacecraft features also appear as sources of low-energy electrons either by photoelectron release or secondary electron production from the spacecraft surface. These sources are hard to quantify theoretically and we only provide a qualitative description of them here. Future work will aim to characterise these more precisely and calibrate the data accordingly. For now, the features described here should be noted and the effects taken into account when using EAS data for analysis.

Blockages – Several features of the spacecraft are visible as reduced count levels in the FoV of EAS:

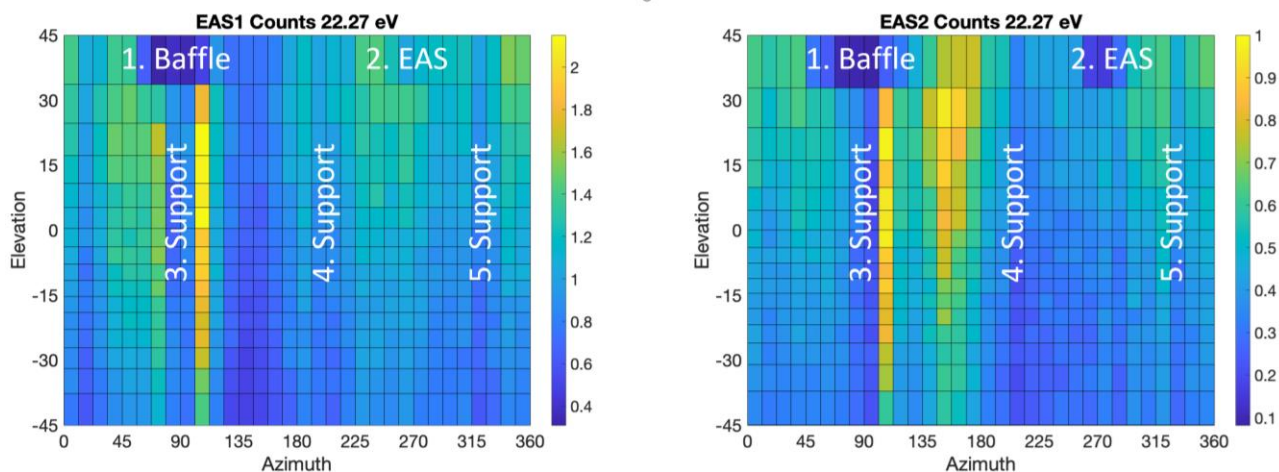


Figure 1: 22.27 eV energy electron counts in the EAS FoV. Blockages are labelled corresponding to Table 1.

Table 1: EAS FoV blockages

Structure	Azimuths		Elevations		Energies		Comments
	EAS1	EAS2	EAS1	EAS2	EAS1	EAS2	
1. Baffle	56.25	45	33.68	32.88	All	All	
	-	-	-	-			
	123.75	123.75	45	45			
2. EAS	247.5	247.5	33.68	32.88	All	All	
	-	-	-	-			
	292.5	292.5	45	45			
3. Support structures	78.75	78.75	All	All	All	All	
	-	-					
	101.25	101.25					
4. Support structures	202.5	202.5	All	All	All	All	
	-	-					
	212.75	212.75					
5. Support structures	326.25	326.25	All	All	All	All	
	-	-					
	337.5	337.5					

Counts in the energy, azimuth and elevations described in Table 1 are lower than the surrounding values due to the blockages. These bins should not be used for analysis if at all possible. If they must be used, then an ad-hoc calibration will be required. These structures may also become sources for secondary electrons and photoelectrons at energies below about 15 eV.

The support structures (3, 4, 5 in Table 1) are included in the calibration of the instrument and so when using the distribution function data products, the impact of these blockages on the resulting data should be small.

Photoelectrons and secondary electron sources – Several features of the spacecraft are visible as increased count levels in the FoV of EAS, especially at low energy:

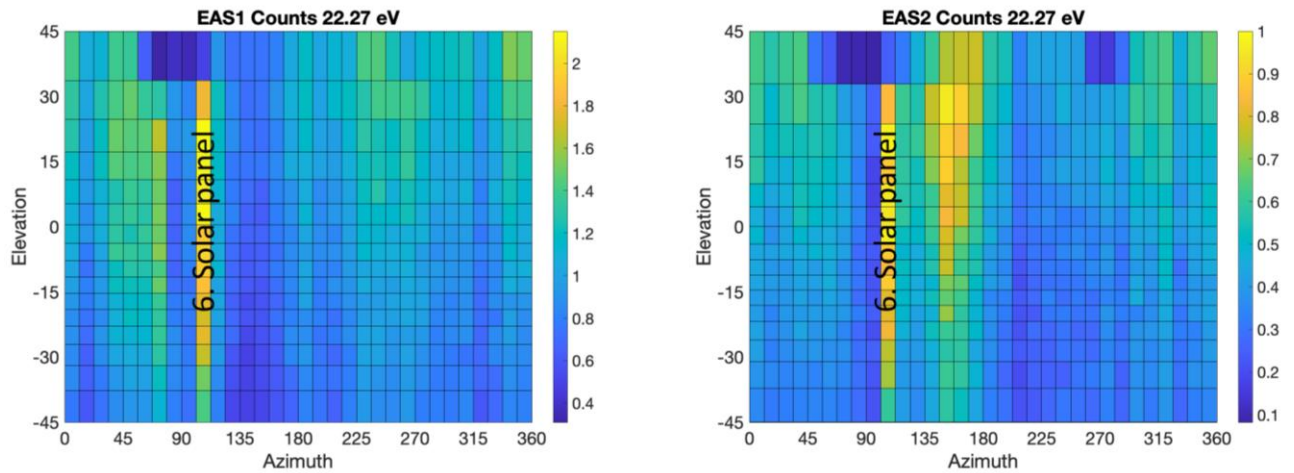


Figure 2: 22.27 eV energy electron counts in the EAS FoV. Sources are labelled corresponding to Table 2.

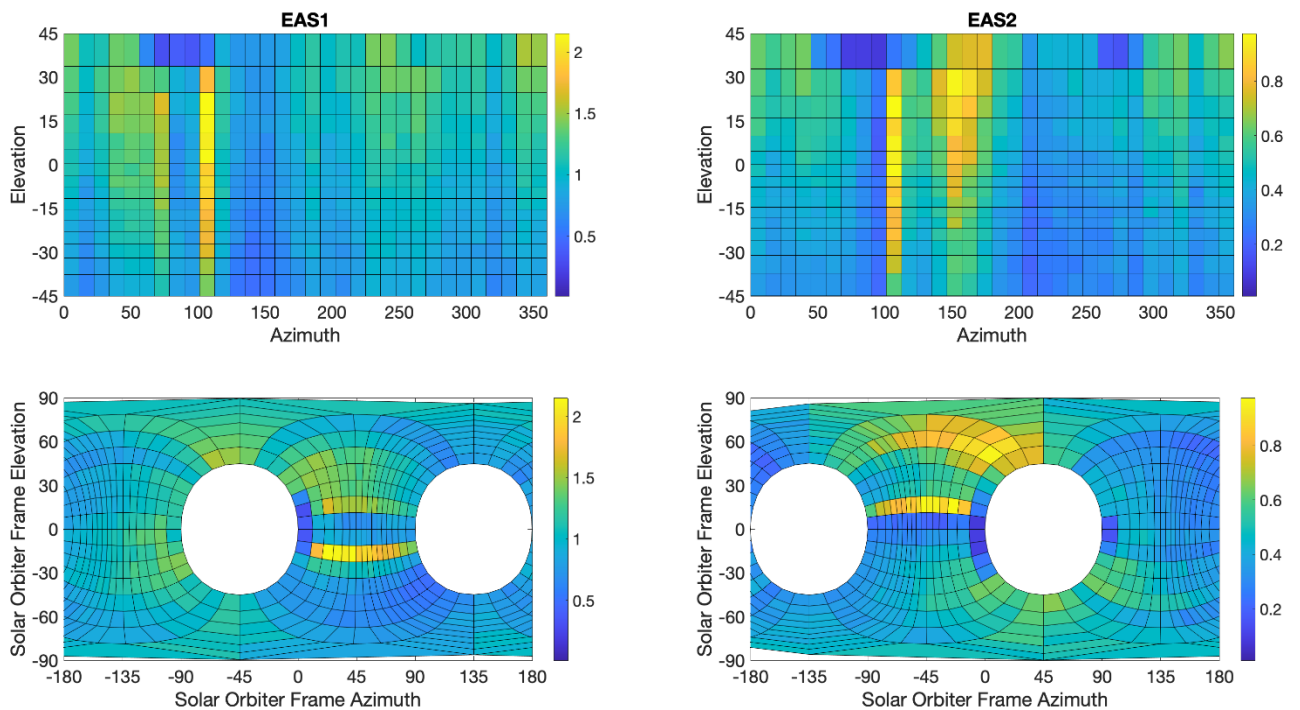


Figure 3: Mapping of 22.27 eV energy electron counts in the EAS FoV in sensor frames (top panels) into the spacecraft frame.

Table 2: EAS FoV spacecraft sources

Structure	Azimuths		Elevations		Energies		Comments
	EAS1	EAS2	EAS1	EAS2	EAS1	EAS2	
6. Solar panels	101.25	101.25	All	All			
	-	-					
	112.5	112.5					
7. High-gain antenna							
8. Boom							

## 4.2 Energy range

The energy range used, and the extent of individual energy bins for a given set of observations are contained within the SWA EAS cdf files.

## 4.3 The ‘Sawtooth’

Counts and also the derived phase space densities of EAS data show a systematic effect where the even numbered energy steps consistently record higher counts than neighbouring odd numbered energy steps. The result is a ‘sawtooth’ distribution in the counts as a function of energy.

This behaviour is not fully understood, but relates to the direction of change of voltage applied to the deflector plates and hemispheres of the top-hat detectors. Even energy steps are recorded with an upwards sweeping voltage and odd steps with the downwards sweep in energy. Lower energy levels are more strongly affected than the higher energies and there is a directional dependence to the effect too.

We will now discuss detailed features of this effect discovered in the commissioning of EAS so far:

1. Energy dependence;
2. Direction dependence;
3. Splitting even and odd energies;

The overall result is that we recommend extreme caution when analysing the count and distribution function data from EAS at the current time. Comparing neighbouring energy levels is subject to a large systematic error that has not been fully quantified or understood. However, we can offer the following advice / recommendations if analysing these data:

1. Separate even and odd energy steps and use each separately for a lower resolution data product;
2. Even energy steps (those with higher counts) are more likely to be an accurate representation of the plasma than the lower count level. This is because the

instrument only operates at maximum counting efficiency when the voltages applied to all surfaces match closely. Any mismatch will result in lower counts, so we can assume that higher counts represent better performance;

3. Energy steps above about 30 eV only display a very minor effect, so studies of strahl and superthermal electrons should be possible at the native resolution of the instrument, however any close comparison of distribution function or counts across different energy steps should proceed with caution.

## 5 Onboard Moments

### 5.1 Executive Summary Statement:

Users should note that all ‘onboard’ moments in the EAS L1 and L2 files are generated by an onboard algorithm which depends on use of an accurate measure of the spacecraft potential, and cannot account for the presence of electrons of spacecraft origin within the calculation. At present both these aspects are under assessment by the SWA/EAS team (see discussions in Section 4 above), and very limited corrections have been applied. Some of these effects are described below, but in general the user should exercise extreme caution in use of this data to draw strong scientific conclusions. The density data may have some useful indication of large scale variations, but the higher order moments likely have large offsets between sensors which have not been removed. We hope to be able to produce more accurate values in later update releases.

### 5.2 General discussion of EAS moments

Note first that the conversion from counts,  $C_{S,i,j,k}$ , to distribution function,  $f_{S,i,j,k}$ , is given by:

$$f_{S,i,j,k} = \frac{C_{S,i,j,k}}{v_{S,i}^4 G_S T}$$

Where S represents the sensor number (S = 1,2), (i, j, k) are the indices over the energy (64 levels), elevation (16 bins) and azimuth (32 bins) measurement samples,  $v_{S,i}$  is the velocity associated with a given energy bin  $i$ ,  $G_S$  the *geometrical factor* of each sensor (units of  $(sr * m^2 eV)/eV$ ) and  $T$  is the *accumulation time* (which for the nominal EAS cadence of 1 sec would be  $T = 1/((64+1)*16) = 0.96 ms$ , assumed to be the same for both sensors).

The values for  $f_{S,i,j,k}$  here should be expressed in physical units  $\left[ \frac{m^4}{s^4} \frac{sr \cdot m^2 \cdot eV}{eV} s \right]^{-1} = 1/(m^6 sr/s^3)$ .

The phase space volume for a given pixel should be:

$$\Delta v = v_{S,i}^2 \Delta v_{S,i} \cos \theta_j \Delta \phi_k \Delta \theta_j$$

Where  $\Delta v_{S,i}$  is the width of the energy channel (assumed sensor dependent),  $\Delta\theta_j$  and  $\Delta\phi_k$  are the widths of the elevation and azimuth angle sectors respectively (both assumed here to be sensor independent).

Hence we can define the contribution of a given element to the number density as:

$$dn_{S,i,j,k} = f\Delta v = \frac{C_{S,i,j,k}}{v_{S,i}^4 G_S T} v_{S,i}^2 \cos\theta_j \Delta v_{S,i} \Delta\theta_j \Delta\phi_k$$

For SWA/EAS we group and sum appropriate combinations of sensor/measurement bin elements to construct a set of partial moments over a set of 3 energy ranges and 2 angular ranges per sensor, and thus return  $3 * 2 * 2$  values for each of the density moments. This is done by defining ‘masks’ to the data onboard such that only the counts from a specified region of phase space contribute to the partial moment sum. Thus recovery of the set of full moments would need to be a further summation over an appropriate combination of the partial moments. The 3 energy range masks can be defined to be:

- i)  $M_{lowE,i}$ : This is 1 for the low energy range (nominally  $< 10$  eV), 0 otherwise;
- ii)  $M_{corE,i}$ : This is 1 for the core energy range (nominally  $10 < E < 68$  eV), 0 otherwise;
- iii)  $M_{strE,i}$ : This is 1 for the strahl energy range (nominally  $> 68$  eV), 0 otherwise;

(Note there may be a small issue with the masks if the energy bins are not the same for the 2 sensors, but hopefully this is a second order effect that can be handled later?)

The 2 angular range masks for each sensor can be defined as:

- i)  $A_{only,S,j,k}$ : containing the solid angle of space observed by sensor S only;
- ii)  $A_{over,S,j,k}$ : containing the solid angle of space observed by sensor S which is also covered by the other sensor;

A typical partial moment might therefore be assembled thus (in this case the density for the EAS1 only region across the core energy range):

$$n(EAS1 \text{ only, core } E) = \sum_{i,j,k} M_{corE,i} A_{only,S=1,j,k} dn_{S=1,i,j,k}$$

A full version of the moments of the kind that is more usual to see from data must then be constructed from an appropriate combination of the partial moments. Note that since there is a region of overlap of the fields of view (which in principle should return the same values from each of the 2 sensors and can be used to check cross calibration), then a full moment can be constructed in 2 ways. For example, assuming the low E range contains only the photo- and secondary electrons, one might assess the density moment can be given by:

$$N(\text{full}) = n(EAS1 \text{ only, core } E) + n(EAS1 \text{ only, strahl } E) + n(EAS2 \text{ only, core } E) + n(EAS2 \text{ only, strahl } E) + n(EAS1 \text{ overlap, core } E) + n(EAS1 \text{ overlap, strahl } E)$$

Or equivalently (in the case of good cross calibration):

$$N(\text{full}) = n(\text{EAS1 only, core E}) + n(\text{EAS1 only, strahl E}) + n(\text{EAS2 only, core E}) + n(\text{EAS2 only, strahl E}) + n(\text{EAS2 overlap, core E}) + n(\text{EAS2 overlap, strahl E})$$

(Note that only 1 of the ‘overlap’ moments needs to be included).

In principle, since all higher order moments are constructed by linear combinations of the masked  $dn_{S,l,j,k}$  (see NR3, Eqns 3 to 26, also reproduced in Appendix A here), all of the full moment set can be reconstructed in this way. The practicalities of this are discussed in the next section.

### 5.3 Practicalities of constructing L2 Moments from L1 onboard partial moments.

Given the above discussion, the biggest issues concerning the construction of a meaningful set of full moments are:

- i) Cross-calibration of the sensor heads;
- ii) Verification that the s/c potential has been correctly applied, and/or adjusting the results accordingly;
- iii) Adjustment of moments to account for inclusion of photo- and secondary-electrons in the various energy and angle ranges used to generate the individual partial moments.

Item (ii) is likely to be a difficult issue as it is preferable that this is correctly handled prior to the calculation of the partial moments onboard by the DPU. At the time of writing, it is not clear that the analysis of either the RPW data or the SWA data has proceeded to the point that this is known to be correctly working, so this issue requires further work outside of this discussion. We therefore proceed with the discussion of moment handling with the assumption that the partial moments returned from the spacecraft do not need further adjustment for the spacecraft potential. We can check results of compiling full moments against RPW and PAS data as appropriate and available.

#### 5.3.1 Cross calibration of the sensor heads.

As a matter of design, the partial moments from the overlap regions should in principle match between the 2 heads, since they are sampling the same portion of sky. In practice, this is not exact since the 2 heads are known to be differently affected by access to photo-electrons and secondary electrons. This issue (iii) above, is not yet fully categorized and so is not at present corrected in the EAS moments data. Nevertheless, if we assume that these effects are confined to the low-energy range, then we might expect the overlap moment calculations for the overlap-core-halo and overlap-strahl regions to match, although the latter might be less useful due to anyway low-count rates at those energies.

However, we know that for the initial part of the cruise phase (data released to date) we have a substantial mismatch in the counting efficiencies of the 2 sensors, with EAS2 counting rather less efficiently than EAS1. This can be seen in the plots of long term count rates and indeed in the moment calculations themselves. Figure 4 shows the long term hourly averaged count rate evolution for the count rates in the core-halo energy range (8 to 68 eV, left hand column of plots) and strahl energy range (> 68 eV, right hand column) as a function of hours since June 8<sup>th</sup>. The upper panel in both columns shows the radial

distance of the spacecraft from the Sun, the second panel shows the hourly average count rate (blue for EAS1, red for EAS2), and the third panel shows the same data corrected for the distance factor. The final panel shows the ration of counts between EAS1 and EAS2. From the latter panels it is clear that there was initially some evolution of the ratio, but this has settled down to a ratio of  $\sim 2.36$  for the core-halo energies and  $\sim 1.87$  for the strahl energies (cf overall ratio of 2.43 for the full energy range and 2.65 for the low energy range, not shown here).

Similar results come about from a direct comparison of the density moments in the overlap ranges. Figure 5 shows the overlap density partial moments from a single day (18<sup>th</sup> September 2020). The top panel shows the EAS1 and EAS2 low energy overlap

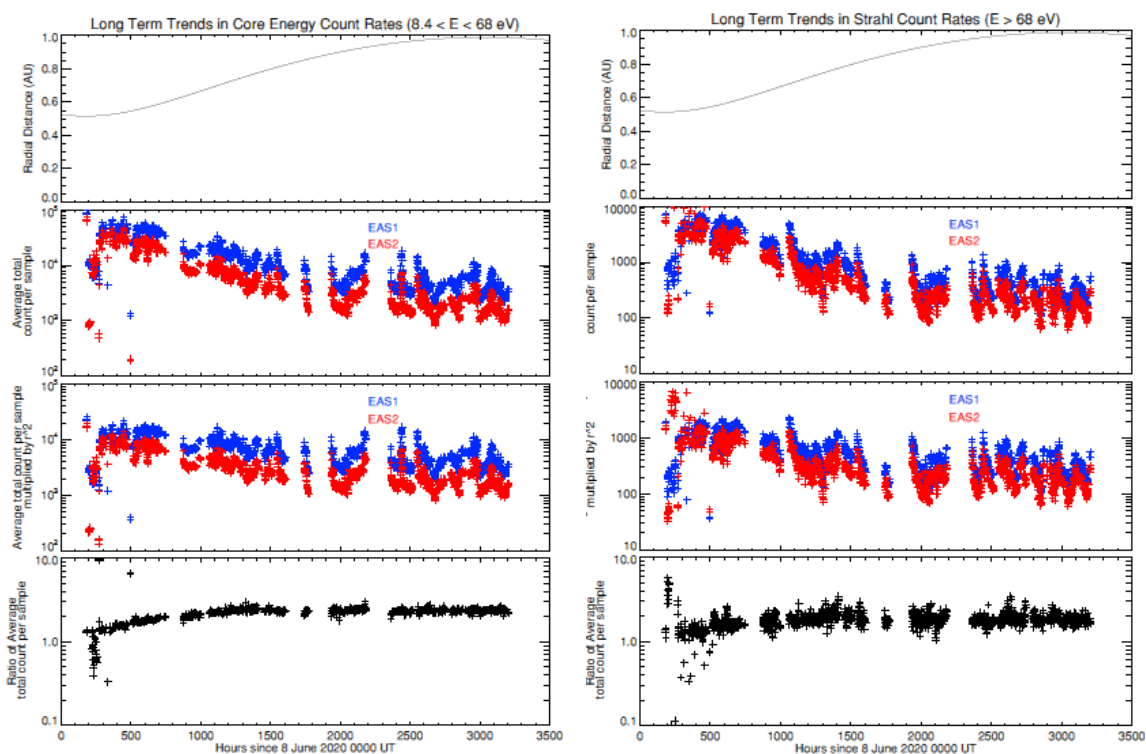


Figure 4: Long term evolution of EAS1 and EAS2 count rates in the core-halo and strahl energy ranges.

moments (red and pink respectively), the core-halo overlap energy moments (dark and light blue respectively), and the strahl overlap moments (green and yellow respectively). Interestingly although all are at different values, they all show the same general variations. The lower panel of Figure 5 shows the relevant ratios between EAS1 and EAS2 for the 3 energy ranges (low energy range in red, core-halo in blue and strahl in green). Although there is a daily variation here, the average levels are not dissimilar from the ratios of the count rates for this period, as derived from Figure 4. This is also evident from the scatter plot of EAS1 vs EAS2 partial density data shown in the right hand plot of Figure 5. The gradients of the line are broadly consistent with the efficiencies derived above.

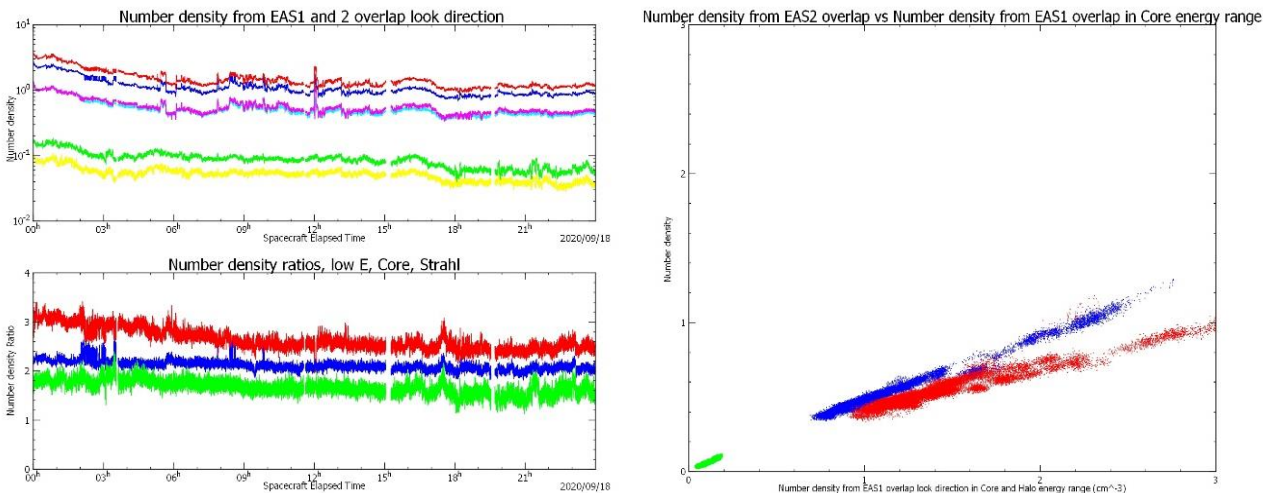


Figure 5: Left top panel –plot of overlap region partial moments for 18/09/2020 showing EAS1 and EAS2 low energy density (red and pink respectively), core-halo density (dark and light blue) and strahl density (green and yellow); Lower left panel shows the ratio of EAS1 to EAS2 partial densities in the low energy (red) core-halo (blue) and strahl (green) ranges. The right hand plot shows a scatter plot of the same data.

Given that we expect the low energy range count rates may indeed be variable depending on the access photo- and secondary electrons have to each of the 2 sensors, and that the strahl energy range may be less reliable due to low counts in this range, we conclude as a working hypothesis that we should apply a relative inter-calibration of counting efficiency,  $E_{12}$ . For the period shown here its value is  $\sim 2.36$ .

### 5.3.2 Density Moment

Given the relationship of every moment to the value of  $dn_{S,i,j,k}$  (see Appendix A), if we inter-calibrate the partial moments by replacing  $dn_{2,i,j,k}$  with  $E_{12} * dn_{2,i,j,k}$  with to account for the lower counting efficiency, we see that most of the EAS2 partial moments need to be increased by this factor since the constant  $E_{12}$  can be simply taken outside of the individual summations. Thus we might construct the full density moment (with reference to the above) for the L2 files by calculating:

$$N (full) = n(EAS1 \text{ only, core } E) + n(EAS1 \text{ only, strahl } E) + E_{12} * (n(EAS2 \text{ only, core } E) + n(EAS2 \text{ only, strahl } E)) + n(EAS1 \text{ overlap, core } E) + n(EAS1 \text{ overlap, strahl } E)$$

Or equivalently (now there should be reasonable cross calibration):

$$N (full) = n(EAS1 \text{ only, core } E) + n(EAS1 \text{ only, strahl } E) + E_{12} * (n(EAS2 \text{ only, core } E) + n(EAS2 \text{ only, strahl } E)) + n(EAS2 \text{ overlap, core } E) + n(EAS2 \text{ overlap, strahl } E)$$

(Note again that only 1 of the ‘overlap’ moments needs to be included, which might make the former formula preferable as it involves fewer ‘corrected’ parameters).

### 5.3.3 Velocity Moments

For the velocity moment, we need to fold back in the partial density moments to correctly weight the contributions (the moment calculation is done as a momentum flux, not a velocity). In addition, it appears that a correction to reverse all the z-components of velocity in the sensor frames is first needed, due to the difference in treatment of elevations and azimuths in terms of look-direction vs arrival direction. So inclusion of this correction, and the rotation of the measurements from the 2 sensors into a common frame, implies the use of matrix operations:

$$M_1 = R_1 \# \begin{pmatrix} 1 & 0 & 0 \\ 0 & 1 & 0 \\ 0 & 0 & -1 \end{pmatrix} ; M_2 = R_2 \# \begin{pmatrix} 1 & 0 & 0 \\ 0 & 1 & 0 \\ 0 & 0 & -1 \end{pmatrix}$$

Unfortunately, comparison of the overlap region velocities shows that, at present, the absence of spacecraft potential corrections and removal of the effects of electrons of spacecraft origins has a significant effect on the velocity moments from each head. Figure 6 below shows the individual velocities in the overlap partial moment range for core energies (left hand plot) and strahl energies. At the top of both sets of plots is the cross-calibrated density. The next 3 panels show the overlap velocity components ( $V_x$ ,  $V_y$ ,  $V_z$  in the spacecraft reference frame) from the 2 sensors (EAS1 in blue, EAS2 in red). For clarity these data have been smoothed using a 60 sec boxcar sliding average. From these it is clear that there are significant offsets in velocity (explicitly shown in the bottom panels) between the 2 sensors. These are presumably due to the presence of electrons generated from spacecraft surfaces local to the sensor which provide a different offset at each sensor. Nevertheless, the variations between the 2 sensors track well, such that this offers some hope that these offsets can be removed from the data product prior to assembly of the full velocity moment. However, at present this correction is not fully assessed or in any way applied.

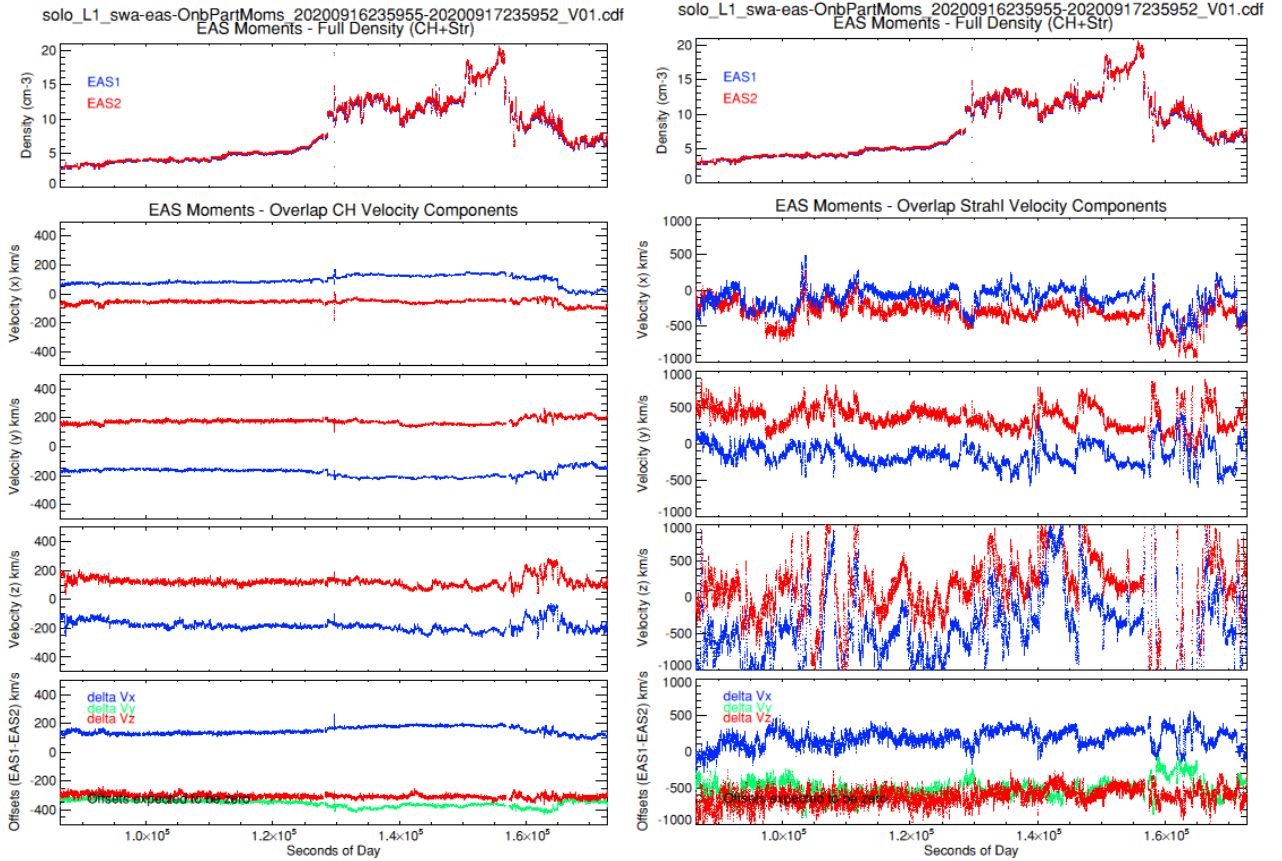


Figure 6: Partial velocity moments from EAS1 (blue) and EAS2 (red) in the overlap region for core-halo energies (left) and strahl energies (right). In principle these are derived from a sampling of a common FoV, so ideally would show the same values. The evident offsets (shown also in the bottom panels) are due to spacecraft origin electrons which are known to be measured very differently for each head.

Then the 2 calculations that could return the full velocity moment for the L2 files would be:

$$\begin{aligned}
 V(\text{full}) = & N(\text{full})^{-1} * \{n(\text{EAS1 only, core E}) * M_1 \# V(\text{EAS1 only, core E}) \\
 & + n(\text{EAS1 only, strahl E}) * M_1 \# V(\text{EAS1 only, strahl E}) \\
 & + E_{12} * (n(\text{EAS2 only, core E}) * M_2 \# V(\text{EAS2 only, core E}) \\
 & + n(\text{EAS2 only, strahl E}) * M_2 \# V(\text{EAS2 only, strahl E})) \\
 & + n(\text{EAS1 overlap, core E}) * M_1 \# V(\text{EAS1 overlap, core E}) \\
 & + n(\text{EAS1 overlap, strahl E}) * M_1 \# V(\text{EAS1 overlap, strahl E})\}
 \end{aligned}$$

Or equivalently:

$$\begin{aligned}
 V(\text{full}) = & N(\text{full})^{-1} * \{n(\text{EAS1 only, core E}) * M_1 \# V(\text{EAS1 only, core E}) \\
 & + n(\text{EAS1 only, strahl E}) * M_1 \# V(\text{EAS1 only, strahl E}) \\
 & + E_{12} * (n(\text{EAS2 only, core E}) * M_2 \# V(\text{EAS2 only, core E})
 \end{aligned}$$

$$\begin{aligned}
 &+ n(\text{EAS2 only, strahl } E) * M_2 \# V(\text{EAS2 only, strahl } E) \\
 &+ n(\text{EAS2 overlap, core } E) * M_2 \# V(\text{EAS2 overlap, core } E) \\
 &+ n(\text{EAS2 overlap, strahl } E) * M_2 \# V(\text{EAS2 overlap, strahl } E))\}
 \end{aligned}$$

Again, the former formula involves fewer 'corrected parameters.

### 5.3.4 Heat Flux Vector Moments

As was the case for the velocity moment, it appears that a correction to reverse all the z-components of heat flux in the sensor frames is first needed, due to the difference in treatment of elevations and azimuths in terms of look-direction vs arrival direction. So inclusion of this correction, and the rotation of the measurements from the 2 sensors into a common frame, again implies the use of matrix operations:

$$M_1 = R_1 \# \begin{Bmatrix} 1 & 0 & 0 \\ 0 & 1 & 0 \\ 0 & 0 & -1 \end{Bmatrix} ; \quad M_2 = R_2 \# \begin{Bmatrix} 1 & 0 & 0 \\ 0 & 1 & 0 \\ 0 & 0 & -1 \end{Bmatrix}$$

Then the 2 calculations that could return the full heat flux moment for the L2 files would be:

$$\begin{aligned}
 H(\text{full}) = & \{ M_1 \# H(\text{EAS1 only, core } E) + M_1 \# H(\text{EAS1 only, strahl } E) \\
 & + E_{12} * (M_2 \# H(\text{EAS2 only, core } E) + M_2 \# H(\text{EAS2 only, strahl } E)) \\
 & + M_1 \# H(\text{EAS1 overlap, core } E) + M_1 \# H(\text{EAS1 overlap, strahl } E) \}
 \end{aligned}$$

Or equivalently

$$\begin{aligned}
 H(\text{full}) = & \{ M_1 \# H(\text{EAS1 only, core } E) + M_1 \# H(\text{EAS1 only, strahl } E) \\
 & + E_{12} * (M_2 \# H(\text{EAS2 only, core } E) + M_2 \# H(\text{EAS2 only, strahl } E) \\
 & + M_2 \# H(\text{EAS2 overlap, core } E) + M_2 \# H(\text{EAS2 overlap, strahl } E)) \}
 \end{aligned}$$

Again, the former formula involves fewer 'corrected' parameters.

Again, the accuracy of the final heat flux moment will be critically dependent on removing the artefacts due to spacecraft electrons, although as these are generally at lower energies they might be expected to have smaller effects on these higher order moments. However this has not been addressed by the EAS team at this point in time.

### 5.3.5 Pressure Moments

The L1 partial moments for pressure each contain the 6 values for P<sub>XX</sub>, P<sub>XY</sub>, P<sub>XZ</sub>, P<sub>YY</sub>, P<sub>YZ</sub>, P<sub>ZZ</sub> in the individual sensor frame. The partial tensor for each sensor/energy/FoV range is assembled as:

$$P = \begin{bmatrix} P_{XX} & P_{XY} & P_{XZ} \\ P_{XY} & P_{YY} & P_{YZ} \\ P_{XZ} & P_{YZ} & P_{ZZ} \end{bmatrix}$$

As was the case for the velocity moment, it appears that a correction to reverse all the P<sub>z</sub>-components of heat flux in the sensor frames is first needed, due to the difference in

treatment of elevations and azimuths in terms of look-direction vs arrival direction. So inclusion of this correction, and the rotation of the measurements from the 2 sensors into a common frame, again implies the use of matrix operations:

$$M_1 = R_1 \# \begin{pmatrix} 1 & 0 & 0 \\ 0 & 1 & 0 \\ 0 & 0 & -1 \end{pmatrix} ; \quad M_2 = R_2 \# \begin{pmatrix} 1 & 0 & 0 \\ 0 & 1 & 0 \\ 0 & 0 & -1 \end{pmatrix}$$

The conversion to the spacecraft frame is then given by:

$$P'_1 = M_1 P_1 M_1^{-1} ; \quad P'_2 = M_2 P_2 M_2^{-1}$$

Then the 2 calculations that could return the full pressure tensor for the L2 files would be:

$$\begin{aligned} \underline{P}'(full) = & \{ P'_1(EAS1 \text{ only, core } E) + P'_1(EAS1 \text{ only, strahl } E) \\ & + E_{12} * (P'_2(EAS2 \text{ only, core } E) + P'_2(EAS2 \text{ only, strahl } E)) \\ & + P'_1(EAS1 \text{ overlap, core } E) + P'_1(EAS1 \text{ overlap, strahl } E) \} \end{aligned}$$

Or equivalently

$$\begin{aligned} \underline{P}'(full) = & \{ P'_1(EAS1 \text{ only, core } E) + P'_1(EAS1 \text{ only, strahl } E) \\ & + E_{12} * (P'_2(EAS2 \text{ only, core } E) + P'_2(EAS2 \text{ only, strahl } E)) \\ & + P'_2(EAS2 \text{ overlap, core } E) + P'_2(EAS2 \text{ overlap, strahl } E) \} \end{aligned}$$

Again, the former formula involves fewer 'corrected' parameters.

Again, the accuracy of the final pressure moment will be critically dependent on removing the artefacts due to spacecraft electrons, although as these are generally at lower energies they might be expected to have smaller effects on these higher order moments. However, this has not been addressed by the EAS team at this point in time.

## 6 Burst Mode

The EAS BM is a high time resolution data product which is derived by 'steering' the EAS sensors to take a sampling of the full 3D velocity distribution function which can be recast into a full pitch angle distribution (PAD). It thus has all the same caveats as described for the 3D data product in section 4.

In addition, users should note that the steering algorithm makes use of a magnetic field unit vector transmitted on board the spacecraft from the MAG sensor (see NR4). Thus the accuracy of the pitch angles assigned to the EAS measurements depend on the accuracy of the magnetometer offsets for any given day. The EAS team intends to create a L2 data product which has the corrected, ground validated magnetic field vector as its basis, but this has not been enacted for first release. Users of this data should therefore take care to rebin the data according to the released field vector from the MAG team.

## Appendix A – Moment Calculations

Given  $dn_{S,i,j,k} = f\Delta v = \frac{C_{S,i,j,k}}{v_{S,i}^4 G_{ST}} v_{S,i}^2 \cos \theta_j \Delta v_{S,i} \Delta \theta_j \Delta \varphi_k$

one can perform moments calculation as follows:

$$n = \sum_{i,j,k} dn_{i,j,k} \quad [eq.1]$$

$$nV_x = \sum_{i,j,k} v_i \cos \theta_j \cos \varphi_k dn_{i,j,k} \quad [eq.2]$$

$$nV_y = \sum_{i,j,k} v_i \cos \theta_j \sin \varphi_k dn_{i,j,k} \quad [eq.3]$$

$$nV_z = \sum_{i,j,k} v_i \sin \theta_j dn_{i,j,k} \quad [eq.4]$$

$$\Pi_{xx} = m \sum_{i,j,k} (v_i \cos \theta_j \cos \varphi_k)^2 dn_{i,j,k} \quad [eq.5]$$

$$\Pi_{xy} = m \sum_{i,j,k} (v_i \cos \theta_j \cos \varphi_k)(v_i \cos \theta_j \sin \varphi_k) dn_{i,j,k} \quad [eq.6]$$

$$\Pi_{xz} = m \sum_{i,j,k} (v_i \cos \theta_j \cos \varphi_k)(v_i \sin \theta_j) dn_{i,j,k} \quad [eq.7]$$

$$\Pi_{yy} = m \sum_{i,j,k} (v_i \cos \theta_j \sin \varphi_k)^2 dn_{i,j,k} \quad [eq.8]$$

$$\Pi_{yz} = m \sum_{i,j,k} (v_i \cos \theta_j \sin \varphi_k)(v_i \sin \theta_j) dn_{i,j,k} \quad [eq.9]$$

$$\Pi_{zz} = m \sum_{i,j,k} (v_i \sin \theta_j)(v_i \sin \theta_j) dn_{i,j,k} \quad [eq.10]$$

$$Q_x = \frac{m}{2} \sum_{i,j,k} v_i^2 (v_i \cos \theta_j \cos \varphi_k) dn_{i,j,k} \quad [eq.11]$$

$$Q_y = \frac{m}{2} \sum_{i,j,k} v_i^2 (v_i \cos \theta_j \sin \varphi_k) dn_{i,j,k} \quad [eq.12]$$

$$Q_z = \frac{m}{2} \sum_{i,j,k} v_i^2 (v_i \sin \theta_j) dn_{i,j,k} \quad [eq.13]$$

Being:

$$v_i^2 = (v_i \cos \theta_j \cos \varphi_k)^2 + (v_i \cos \theta_j \sin \varphi_k)^2 + (v_i \sin \theta_j)^2 \quad [\text{eq.14}]$$

Furthermore, moving the second order moments in the plasma reference frame:

$$P_{xx} = m \sum_{i,j,k} [v_i \cos \theta_j \cos \varphi_k - V_x]^2 dn_{i,j,k} \quad [\text{eq.15}]$$

$$P_{xy} = m \sum_{i,j,k} [v_i \cos \theta_j \cos \varphi_k - V_x][v_i \cos \theta_j \sin \varphi_k - V_y] dn_{i,j,k} \quad [\text{eq.16}]$$

$$P_{xz} = m \sum_{i,j,k} [v_i \cos \theta_j \cos \varphi_k - V_x][v_i \sin \theta_j - V_z] dn_{i,j,k} \quad [\text{eq.17}]$$

$$P_{yy} = m \sum_{i,j,k} [v_i \cos \theta_j \sin \varphi_k - V_y]^2 dn_{i,j,k} \quad [\text{eq.18}]$$

$$P_{yz} = m \sum_{i,j,k} [v_i \cos \theta_j \sin \varphi_k - V_y][v_i \sin \theta_j - V_z] dn_{i,j,k} \quad [\text{eq.19}]$$

$$P_{zz} = m \sum_{i,j,k} [v_i \sin \theta_j - V_z]^2 dn_{i,j,k} \quad [\text{eq.20}]$$

Only for completion purposes, given:

$$w_i^2 = (v_i \cos \theta_j \cos \varphi_k - V_x)^2 + (v_i \cos \theta_j \sin \varphi_k - V_y)^2 + (v_i \sin \theta_j - V_z)^2 \quad [\text{eq.21}]$$

it is then possible, but actually not required and then not computed, to obtain also the third order moment in the plasma reference frame as follows:

$$H_x = \frac{m}{2} \sum_{i,j,k} w_i^2 [v_i \cos \theta_j \cos \varphi_k - V_x] dn_{i,j,k} \quad [\text{eq.22}]$$

$$H_y = \frac{m}{2} \sum_{i,j,k} w_i^2 [v_i \cos \theta_j \sin \varphi_k - V_y] dn_{i,j,k} \quad [\text{eq.23}]$$

$$H_z = \frac{m}{2} \sum_{i,j,k} w_i^2 [v_i \sin \theta_j - V_z] dn_{i,j,k} \quad [\text{eq.24}]$$



## Appendix B: Abbreviations

Abbreviation	Meaning
EAS	Electron Analyser System
MCP	Micro-Channel Plate
SWA	Solar Wind Analyser
VDF	Velocity Distribution Function